A single-point method to quantitatively diagnose the magnetotail flapping motion

Z. J. Rong[1, 2, 3], C. Zhang[1, 2], Lucy Klinger [4], Y. Wei[1, 2, 3], C. Shen[5], and W. X. Wan[1, 2, 3]

[1]Key Laboratory of Earth and Planetary Physics, Institute of Geology and Geophysics, Chinese Academy of Sciences, Beijing, China

[2]College of Earth Science, University of Chinese Academy of Sciences, Beijing, China

[3]Beijing National Observatory of Space Environment, Institute of Geology and Geophysics, Chinese Academy of Sciences, Beijing, China

[4]Beijing International Center for Mathematical Research, Peking University, China

[5]Harbin Institute of Technology, Shenzhen, China

Corresponding author: Z. J. Rong (rongzhaojin@mail.iggcas.ac.cn)

Key Points:

- A single-point method based on magnetic field measurement is developed to quantitatively diagnose the magnetotail flapping motion.
- An application demonstrates that this method can reasonably infer the average flapping parameters during the whole flapping period.
- This method could be applied widely to single-point spacecraft missions in history for studying planetary magnetotail flapping dynamics.

Abstract

Quantitatively estimating magnetotail flapping motion is critical to understanding and characterizing the dynamics of flapping behaviors. Such an estimation could be achieved in principle by the multipoint analysis of spacecraft tetrahedron, e.g. Cluster or MMS mission, but, owing to the inability of single-point measurement to separate the spatial-temporal variation of magnetic field, would be inadequate for a spacecraft. Since single-point missions dominate explorations of planetary magnetotail, we have developed a single-point method based on the magnetic field measurement that quantitatively estimates the parameters of flapping motion, including spatial amplitude, wavelength, and propagation velocity. A comparison with the application of multi-point analysis of Cluster demonstrates that our method can be reasonably be applied to infer the average parameters over a flapping period. Thus, this method could be applied widely to the "big dataset" accumulated by single-point spacecraft missions in order to study magnetotail flapping dynamics.

Plain Language Summary

The oscillation of a magnetotail current sheet, known as the magnetotail flapping motion, plays an important role in dissipating the magnetic field energy stored in a magnetotail. This flapping motion is a fundamental dynamic behavior of a magnetotail, which has been observed widely in the other planets of our solar system, no matter whether the magnetotail is intrinsic (Earth-like) or induced (Venus-like). The comparative study of the planetary magnetotail flapping motion is essential to

understand the flapping mechanism. Unfortunately, single-point measurements of planetary spacecraft are unable to calculate the flapping velocity of tail current sheet directly, which greatly constrains the lucubration of flapping dynamics. To overcome this difficulty, we present a new single-point method, based on the magnetic field measurement and reasonable assumptions, to quantitatively estimate flapping parameters such as spatial amplitude, wavelength, and propagation velocity. A comparison with the multi-point analysis of Cluster tetrahedron shows the validity and reliability of our single-point method as applied to a flapping case of Earth's magnetotail. Thus, our method could be broadly applied to the "big dataset" accumulated by single-point spacecraft missions in history in order to study the flapping dynamics of planetary magnetotails.

1. Introduction

The flapping motion of a magnetotail current sheet is a fundamental dynamic phenomenon in the Earth's magnetotail, which refers to the back and forth motion of a current sheet, and is manifested as multiple crossings of a current sheet by a spacecraft within a short time (e.g. Lui et al., 1978; Sergeev et al., 1998; Speiser & Ness, 1967; Toichi & Miyazaki, 1976).

Quantitatively diagnosing the characteristics of the flapping motion is important to understand flapping behavior and the role it plays in magnetotail dynamics. In the past twenty years, based on the multipoint measurements of the Cluster tetrahedron on the Earth's magnetotail, many studies unambiguously revealed that flapping motions,

being triggered by some sources around the midnight, are able to propagate azimuthally as kink-like waves toward both flanks with velocities of a few tens of kilometers per second, amplitude 1-3 R_E (Earth radius, 6371 km), and wave length 4~8 R_E (e.g. Zhang, et al., 2002, 2005; Sergeev et al., 2003, 2004; Petrukovich et al. 2006; Shen et al., 2008; Rong et al., 2010, 2015a, 2018a; Runov et al., 2005). In addition to the kink-like flapping motion, the magnetotail current sheet sometimes just flaps up and down but does not propagate as waves, as Rong et al. (2015a) reported, this new flapping type is referred to as steady flapping motion. Based on a statistical survey on the two flapping types, Gao et al.(2018) suggested that the up and down motion of steady flapping around the midnight region could induce the kink-like flapping waves that propagate toward both flanks of the magnetotail.

Based on quantitative analysis of kink-like flapping waves, theoretic models proposed different accounts for the flapping mechanism. For example, it might be magnetohydrodynamic ballooning-type waves (Golovchanskaya & Maltsev, 2005); it could be the drift kink mode of current sheet instability (e.g. Karimabadi, et al., 2003a, 2003b; Sitnov et al., 2006; Zelenyi et al., 2009); or it could be interpreted as magnetohydrodynamic waves related to a double-gradient current sheet model (Erkaev et al., 2007).

The magnetotail flapping motions are observed not only in the Earth's magnetotail but also in the magnetotails of other planets, such as Mercury (Zhang et al., 2020), Venus (Rong et al., 2015b), Mars (DiBraccio et al., 2017), and Saturn and Jupiter (Volwerk et al., 2013). To delineate the characteristics of planetary magnetotail

flapping motions is beneficial to understand the general mechanism of the flapping motion. Nonetheless, in contrast to the multipoint measurements of the Cluster tetrahedron, the single-point measurements of planetary spacecraft missions are unable to calculate the moving velocity of the flapping current sheet directly. Therefore, to study the flapping motion of a planetary magnetotail, the major challenge is figuring out how to use single-point measurement to discover flapping properties.

Rong et al. (2015a) presented a single-point method based on the magnetic field measurements to qualitatively diagnose the flapping types and, if a kink-like type, the propagation direction. In studies of the flapping motion of planetary magnetotail, this method has been applied successfully to Earth (Wu et al., 2016), Venus (Rong et al., 2015b), Mars (DiBraccio et al., 2017), and Mercury (Zhang et al., 2020).

As continuation of Rong et al. (2015a), we present here a new method based on the single-point magnetic field measurement to quantitatively estimate the spatial amplitude, wavelength and propagation velocity of the kink-like flapping motion.

The paper is organized as follows. In Section 2, we present our method. In Section 3, we apply the method to a typical kink-like flapping case in the Earth's magnetotail and compare our results with a multi-point analysis of the Cluster. Finally, we give a summary and discussion in Section 4.

2. Method

Before studying the flapping current sheet, we consider the undisturbed current sheet first. The normal of the undisturbed current sheet is **N,** pointing northward. The anti-parallel magnetic field lines on the opposite sides of the current sheet are orientated along direction **L**, which points Earthward. Thus, as shown in Figure 1a, local coordinate (**L**, **M**, **N**) can be set up to describe the field structure of an undisturbed current sheet, where **M**= **N×L**. The local coordinate system is a prerequisite to our method.

Previous studies demonstrate that the magnetic field over the Earth magnetotail current sheet can be well approximated by a 1-D Harris sheet model (Harris, 1962; Thompson et al., 2005; Zhang et al., 2006). The approximation also makes sense in the Venusian magnetotail (Rong et al., 2014) and the Mercury magnetotail (Rong et al., 2018b). Therefore, in local coordinate, we assume that the spatial profile of the magnetic field over the undisturbed magnetotail current sheet can be represented by a Harris sheet model, that is,

$$B_L = B_0 \tanh\left(\frac{z_N - z_0}{L_0}\right) \tag{1}$$

, where, B_0 is the lobe field, z_0 is the location of the sheet center, z_N is the normal distance to the sheet center, and L_0 is the characteristic scale of the sheet.

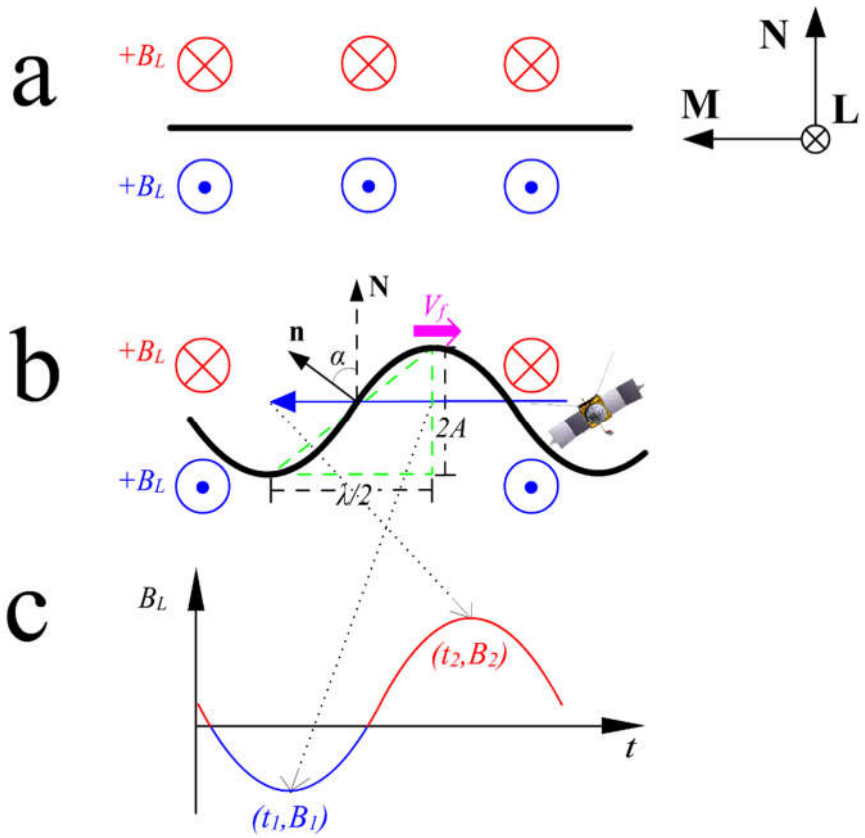

Figure 1. The sketched diagrams show, from top to bottom: (a) the configuration of undisturbed current sheet in the local coordinate ***(L, M, N)****; (b) the kink-like flapping current sheet; and (c) the recorded oscillation of* B_L *component by spacecraft during the flapping period. The current sheet is represented by a thick black line. The kink-like flapping current sheet is assumed to propagate as a wave towards the direction of* $-\boldsymbol{M}$ *with velocity* V_f*, spatial amplitude* A*, and wavelength* λ*. The horizontal blue line represents the relative trajectory of the spacecraft crossing the waves towards the direction of* ***M****. The normal of the crossed current sheet,* ***n****, is tilted from the undisturbed normal* ***N*** *by angle* α*. The recorded* B_L *reaches the trough* B_1 *at time* t_1*, and crest* B_2 *at time* t_2*.*

As seen in Figure 1b and Figure 1c, due to the up-down motion of the current sheet during the flapping period, the spacecraft would record a signal of the oscillated magnetic field. The temporal variation of the oscillated magnetic field can be written as

$$\frac{dB_L}{dt} = \frac{B_0}{L_0}\left[1-\tanh\left(\frac{z_N - z_0}{L_0}\right)^2\right]\frac{dz_N}{dt} \tag{2}$$

148 Considering $\frac{dz_N}{dt} > 0$, when the current sheet is moving downward and vice versa,

149 the up-down moving velocity of current sheet, V_N, can be derived as

150 $$V_N = -\frac{dz_N}{dt} = -\frac{dB_L}{dt}\frac{L_0}{B_0}\left[1-\left(\frac{B_L}{B_0}\right)^2\right]^{-1} \quad (3)$$

151 Note that both L_0 and B_0 are assumed constant during the flapping period.

152 Accordingly, the spatial amplitude of the flapping current sheet can be estimated as

153 $$A = \frac{1}{2}\int_{t_2}^{t_1} V_N dt = -\frac{1}{2}\int_{t_2}^{t_1} \frac{dB_L}{dt}\frac{L_0}{B_0}\left[1-\left(\frac{B_L}{B_0}\right)^2\right]^{-1} dt = \frac{-L_0 B_0}{2}\int_{B_2}^{B_1} \frac{dB_L}{B_0^2 - B_L^2}$$
$$= \frac{L_0}{2}\left[a\tanh\left(\frac{B_2}{B_0}\right) - a\tanh\left(\frac{B_1}{B_0}\right)\right] \quad (4)$$

154 , where t_1 and t_2 are the time when the spacecraft recorded the trough and crest of

155 oscillated B_L during a half-period, while B_1 and B_2 are the corresponding values of B_L,

156 when B_L reaches the trough and crest respectively.

157 As shown in Figure 1b, if the flapping motion can propagate azimuthally as

158 kink-like waves towards -**M**, and the local normal of the crossed current sheet can be

159 evaluated as **n,** then the half wavelength can be roughly estimated as

160 $$\frac{\lambda}{2} = \frac{2A}{\tan\alpha} \quad (5)$$

161 , where α, the tilt angle of the local current sheet, is the angle between **n** and **N**.

162 Accordingly, the propagation speed of the kink-like waves can be roughly

163 estimated as

164 $$V_f = \frac{\lambda}{2(t_2 - t_1)} = \frac{2A}{(t_2 - t_1)\tan\alpha} \quad (6)$$

165

3. Application and Test

To test the validity of our method, we apply it to a magnetotail flapping case observed by the Cluster tetrahedron, so that a comparison with multi-point timing analysis can be made.

In this case, magnetic field data points with 4 s resolution (Balogh et al., 2001) are used in geocentric solar magnetospheric (GSM) coordinate, where +x points toward Sunward, +z points nearly northward and in the plane is constituted by an x-axis and a dipole axis, and +y completes the right-handed system.

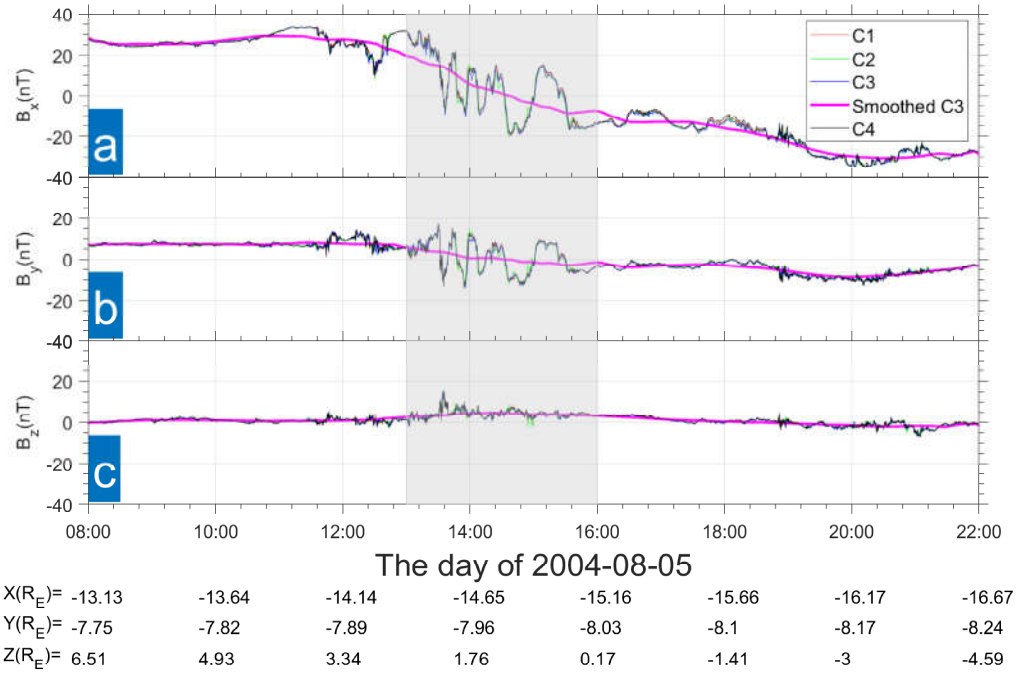

Figure 2. The measured magnetic field by the four spacecraft of Cluster in GSM on 5 August 2004. The interval when the spacecraft experienced a flapping period is shaded. The magenta lines represent the moving average of magnetic field recorded by C3 with span 2 hours. The locations of C3 in GSM are listed in the bottom.

This case occurred on 5 August 2004, during the period of 13:50–16:00, when the Cluster tetrahedron is averagely located at (x = 16.0, y = 9.2, z = 2.7) R_E (R_E = 6371

km, Earth radius). The typical scale of the Cluster tetrahedron is about 1200 km at this time. As shown in Figure 1, each crossing of the tail current sheet, when the x component of magnetic field, B_x, reverses its sign, is marked by a vertical dashed line. Using the multi-point timing analysis of Cluster, Zhang et al. (2005) previously found that the multiple crossings of current sheet are induced by the kink-like flapping motions of the tail current sheet, travelling azimuthally dawnwards with a speed of tens of km/s.

3.1 Local Coordinate of an undisturbed current sheet

It's worthwhile to note that, due to the tail flaring effect of field lines (Fairfield, 1979), the B_y component is positively proportional to the B_x component at the dawn side (Y<0), and it's no surprise to find in Figure 2 that the B_y component oscillates with the same phase as the B_x component. The flaring effect is prominently close to both flanks but negligible around midnight. Thus, to remove the tail flaring effect, we have to set up local coordinate first for an undisturbed tail current sheet.

To set up local coordinate that relies on single-point measurement, knowledge of minimum variance analysis on magnetic field (MVAB) is necessarily required (Sonnerup and Scheible, 1998). By performing MVAB on the sampled magnetic field data points over the crossing of a discontinuity, we can obtain the characteristic directions of the varied magnetic field by solving the magnetic variance matrix $M_{\mu\nu}=\langle B_\mu B_\nu\rangle-\langle B_\mu\rangle\langle B_\nu\rangle$, where the subscripts μ and ν denote the x, y, and z components in a given Cartesian coordinate system, e.g. the GSM coordinate. The

matrix $M_{\mu\nu}$ has three eigenvalues: λ_1, λ_2, and λ_3 ($\lambda_1 \geq \lambda_2 \geq \lambda_3 \geq 0$), and the corresponding eigenvectors **l**, **m**, and **n**. The three eigenvectors are orthogonal and represent the directions of maximum, intermediate, and minimum variance of magnetic field. Taking the magnetotail current sheet as an example, **l** is basically along the local lobe field; **n** is the local normal of the current sheet, and **m**= **n×l** is tangentially to the surface of the current sheet.

With MVAB, there are two ways to construct the local coordinate of a tail current sheet. (1) We could perform MVAB for each crossing of the current sheet, and take the average of **l** for all crossings as **L**. **M** is perpendicular to **L** and the +Z-axis of GSM, i.e. **M**= **L×Z**/| **L×Z** |, and **N= L×M.** This has been adopted in some previous studies (Rong et al., 2015a, 2015b; DiBraccio et al., 2017; Zhang et al., 2020). (2) We could smooth out the fluctuated magnetic field, and perform MVAB on the smoothed field data. In this case, the smoothed field data could be seen as the field of the undisturbed current sheet, and the yielded **l**, **m**, and **n** by MVAB, seen as **L**, **M**, and **N** respectively, could constitute the local coordinate.

We arbitrarily use single-point field measurements of C3 to trial both of these ways. We find that (1) can well remove the flaring effect during the period of crossing current sheet, but the minor positive correlation between B_L and B_M in the local coordinate system is still present when $|B_L|$>20 nT (not shown here). The reason, we found, is caused by the variable configurations of tail field lines, which, as shown in Figure 3, can be indicated by the variable proportion between B_x and B_y during the whole period 08:00-22:00.

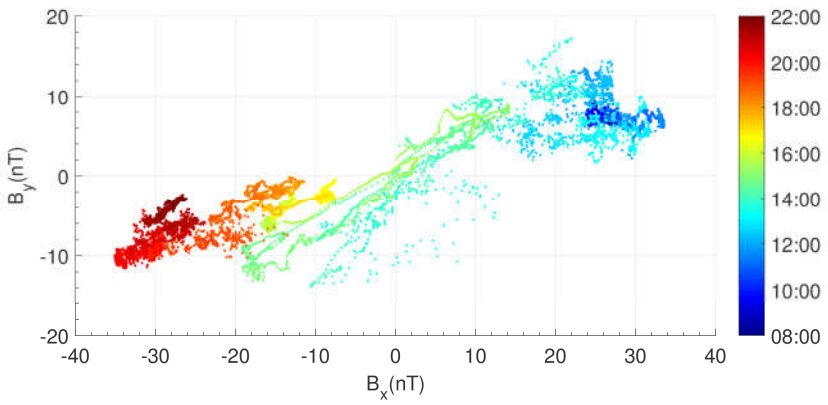

Figure 3. The variation of B_x against B_y during the period 08:00-22:00.

Thus, we could alternatively adopt (2) to set up the local coordinate. Using (2), we have to smooth the field data first. For a flapping period of 20~50 min, we adopt the technique of a moving average with a span of 2 hours to smooth the oscillation of the magnetic field recorded by C3. The moving averaged magnetic field could be seen as the undisturbed magnetic field of the current sheet (see the magenta lines in Figure 1).

With the smoothed field data, we performed MVAB on nested sets of different data interval centered at the current sheet's center (B_L = 0). We chose the interval when the output eigenvectors are insensitive to interval increases, and finally obtained three orthogonal eigenvectors, i.e. **L**= (0.94, 0.33,-0.04), **M**= (0.33, -0.94, -0.02), and **N**= (0.05, 0.00, 1.00), where **N**=**L**×**M**. The ratio of eigenvalues with λ_1: λ_2: λ_3=86: 3: 1 indicates that the yielded eigenvectors are well distinguished.

3.2 Fit with the Harris sheet

Given its local coordinate system (**L**, **M**, **N**) and a smoothed magnetic field (see Figure 4a), we fit the undisturbed current sheet to the Harris sheet model

$B_L = B_0 \tanh\left(\frac{z_N - z_0}{L_0}\right)$. The fitted parameters, with 95% confidence bounds, are B_0= 32.28±0.28 nT, L_0= 3.51±0.06 R_E, and z_0= 7343±87 km. The coefficient of the Adjusted R-square for the fit is 0.97, which indicates the fitting is quite good (the closer one is, the better the fit). Figure 4b shows the spatial distribution of the fitted B_L component.

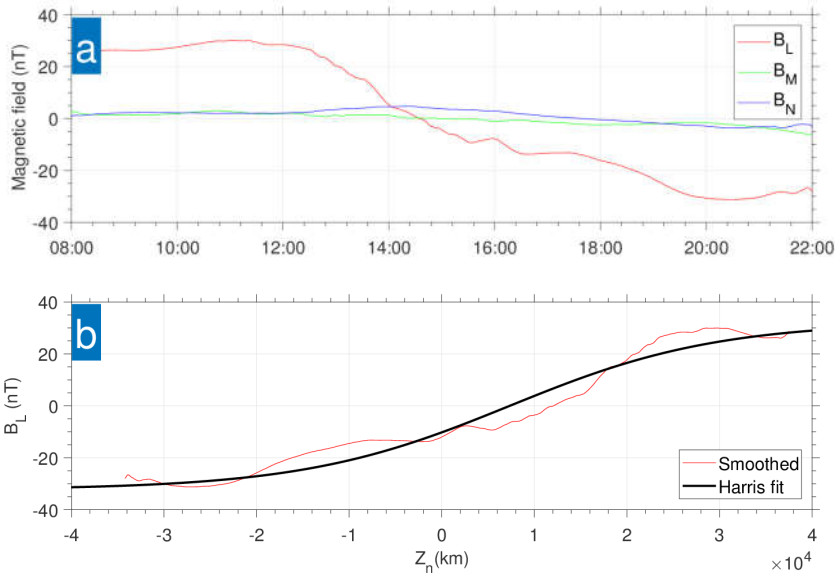

Figure 4. (a) The time series of smoothed magnetic field in the local coordinate of current sheet. (b) The variation of the smoothed B_L component against the normal distance to current sheet center; the black line is the Harris fitting of smoothed B_L component.

3.3 The normal of the local flapping current sheet

Knowledge of the normal of the local current sheet is essential for estimating flapping parameters.

Because the significant time lag of crossing the current sheet in the Cluster tetrahedron favors multi-point timing analysis (Harvey, 1998), as shown in Figure 5a, we consider six crossings of the current sheet that occurred during the period 13:50-15:50, so that a comparison with that timing analysis can be made.

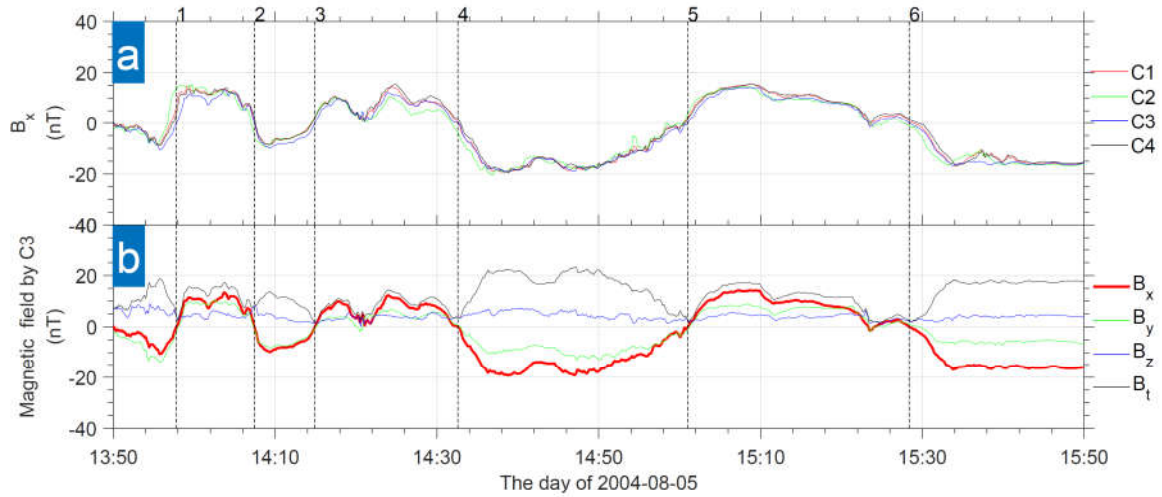

Figure 5. Cluster observations of a flapping tail CS event on 05 August 2004 in GSM coordinate. Panel a shows the recorded B_x component by the four spacecrafts of Cluster. Panel b shows the recorded magnetic field, including its three components in GSM and the field strength, by C3. The dashed lines mark the crossings of tail current sheet.

Timing analysis can derive the normal direction and the associated normal velocity, V_n, of a local current sheet if the sheet is seen as a moving plane. These directions and velocities are tabulated in Table 1. It should be noted that all derived normal directions are dawnwards (n_y<0), which means that the flapping current sheets are travelling dawnward as kink-like waves.

Meanwhile, by employing the MVAB technique (introduced in subsection 3.1), we can also infer the normal orientations that rely on the single-point measurement of C3. The yielded normal orientations, **n**, for the six crossings in GSM and in local coordinate, are tabulated respectively in Table 1. However, in contrast to the timing normal, both **n** and **–n** are valid eigenvectors of MVAB. Thus, one cannot judge the type of flapping or the propagation direction (in the case of kink-like flapping)

279 directly according to the normal MVAB.

280 Given the MVAB normal in local coordinate, Rong et al. (2015a) constructed a
281 parameter k, defined as $k = \mathrm{sig}(n_M \times n_N) \times \mathrm{sig}(\Delta B_L)$, to diagnose the flapping types and
282 ascertain the propagation velocity of flapping waves, where n_M and n_N are the M and
283 N components of **n**, respectively, and $\Delta B_L > 0$, if the polarity of B_L varies from
284 negative to positive and vice versa. Rong et al. (2015) notes that if the flapping
285 motion is propagating toward **M** (+**M**) as kink-like waves**,** the yielded value of k at
286 each crossing of the current sheet would be +1(-1) always; if the flapping motion is
287 just steady flapping, the sequence of k would change its sign alternately. Therefore,
288 the sequence of k can be used to indicate the flapping type and, if the type is kink-like
289 flapping, its propagation direction.

290

291 Table1. Timing and MVAB Analysis on Current Sheet Crossings

MVA results						Timing results	
No.	Time[a]	Δt [b] (s)	λ_2/λ_3[c]	Normal in GSM	Normal in LC[d]	Normal in GSM	V_n[e] (km/s)
1	13:57:47	80	63	-0.64, 0.72, 0.28	-0.37, -0.89, 0.25	0.48, -0.63, -0.61	18
2	14:07:27	56	215	0.64, -0.76, 0.13	0.35, 0.92, 0.16	0.63, -0.69, 0.35	38
3	14:14:55	160	14	-0.46, 0.74, 0.50	-0.21,- 0.86, 0.47	0.19, -0.34, -0.92	37
4	14:32:35	48	21	0.40,-0.56, 0.73	0.16, 0.65, 0.75	0.50, -0.81, 0.32	19
5	15:00:59	96	2	-0.24,0.36, 0.90	-0.14, -0.44, 0.89	0.20, -0.53, -0.82	36
6	15:28:22	48	17	0.44, -0.79, 0.42	0.13, 0.89, 0.44	0.27, -0.71, 0.66	10

292 [a] *The time when C3 crosses the center of the current sheet (B_L=0);*
293 [b] *The length of the used time interval for MVAB, which is centered at the CS center;*

294 [c] *The ratio of λ_2/λ_3; the larger the ratio, the more distinguished the normal* ***n*** *becomes*
295 *from the intermediate direction* ***m****;*
296 [d] *The MVAB normal of C3 in local coordinate (LC);*
297 [e] *The normal velocity of the current sheet inferred by timing analysis.*

298

299 According to the derived MVAB normal in local coordinate (see Table 1), we find
300 that *k*, at each crossing, keeps +1 always, which indicates that the type of flapping
301 motions observed by C3 are kink-like and that these kink-like waves are propagating
302 towards –**M** or dawnward. Evidently, diagnosing flapping motion with the
303 single-point technique of Rong et al. (2015a) is consistent with the results of
304 multiple-point timing analysis.

305 Quantitatively estimating flapping parameters is the main task of this study. We
306 show specific procedures for doing so in the following section.

307 **3.4 The parameters of flapping motion**

308 Having established local coordinate and fitted an undisturbed current sheet to a
309 Harris sheet, we are now in a position to study flapping parameters using the method
310 described in Section 2.

311 To estimate the amplitude of flapping motion via Eq. (4), we have to identify time
312 t_1 and t_2, when the spacecraft recorded the trough and crest of oscillated B_L during a
313 half-period, and obtain the corresponding values of B_L, B_1, and B_2.

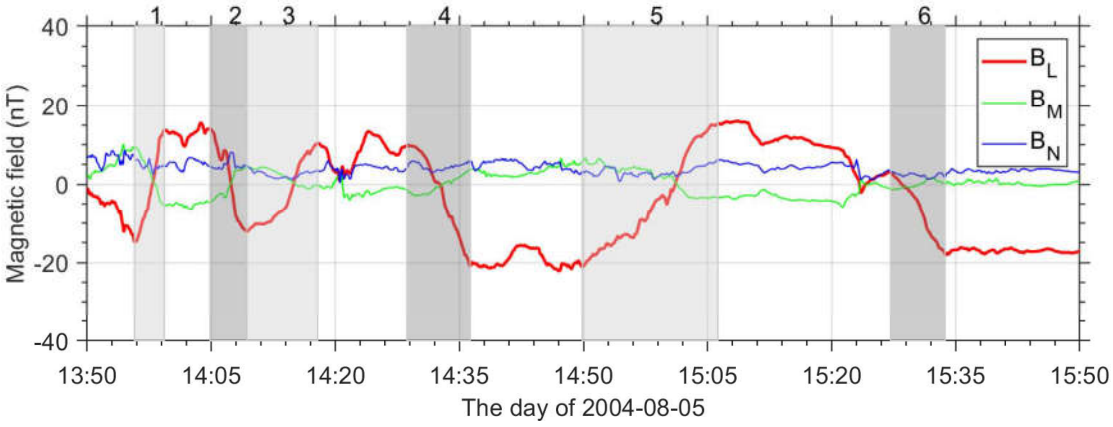

Figure 6. The oscillated magnetic field by C3 in local coordinate. The half-period for each crossing of the current sheet is shaded.

The flapping magnetic field in Figure 6 shows, as expected, that B_L becomes the major field component in the local coordinate system. We have identified the trough and crest of B_L for each crossing, and shaded the corresponding interval of half-period. Note that, due to the irregular waveform of oscillated B_L, the identified half-periods for the neighboring crossing of the current sheet are not adjacent necessarily. Given the identified interval of half-period, and the value of B_L, B_1 and B_2 at trough and crest respectively for each current sheet crossing, we estimate the spatial amplitude using Eq. (4) and tabulate the specific results in Table 2. The estimated results demonstrate that the spatial amplitude during this period is about 1~2 R_E, which is consistent with the typical amplitude reported in previous studies (e.g. Sergeev et al., 2003; Petrukovich et al., 2006; Rong et al., 2018a).

Because the estimated MVAB normal, **n**, may not be strictly coplanar with **M** and **N** as depicted in Figure 1, one has only to consider the projected component of **n** in the MN plane to infer the tilt angle, α, for each crossing of the current sheet. The estimated title angles, in terms of the MVAB and timing normals respectively, are

tabulated in Table 2.

With the derived tilt angle of the MVAB normal, the wavelength and propagation speed for each half-period can be estimated via Eq. (4) and Eq. (5), respectively. As listed in Table 2, we find the estimated wavelength is about 1~3 R_E at crossings 1-3, but can significantly increase up to ~9 R_E at crossing 4, and ~17 R_E at crossing 5, then down to 2.5 R_E at crossing 6. The estimated propagation speed, $V_{f,\,MVAB}$, in tens of km/s, is varied from 13 to 60 km/s, which is comparable to the propagation speed estimated by timing analysis (see "$V_f^{'}$" in Table 2).

Table 2. The estimated flapping parameters for each crossing of current sheet

No.	Interval [a]	Half-period (s)	B_1 (nT)	B_2 (nT)	α_1 [b] (°)	α_2 [b] (°)	A (R_E)	λ (R_E)	$V_{f,\,MVAB}$ [c] (km/s)	$V_{f,\,timing}$ [c] (km/s)	$V_f^{'}$ [d] (km/s)
1	13:55:43-13:59:19	216	-14.9	13.7	77	53	1.7	1.6	24	75	23
2	14:04:51-14:09:19	268	-12.2	14.0	80	66	1.5	1.1	13	32	42
3	14:09:19-14:17:51	512	-12.2	10.4	62	24	1.3	2.7	17	73	92
4	14:28:39-14:36:19	460	-20.9	9.9	41	70	1.9	8.7	60	20	20
5	14:49:51-15:06:15	984	-21.1	15.4	28	36	2.3	17.1	55	41	61
6	15:27:07-15:33:43	396	-18	3.0	64	48	1.3	2.5	20	37	13

[a] *The identified interval of half-period for each crossing of the current sheet.*

[b] *The tilt angle of current sheet. α_1 (α_2) is the angle between the MVAB normal (timing normal) and* ***N****.*

[c] *$V_{f,\,MVAB}$ ($V_{f,\,timing}$) is the propagation speed estimated via Eq.(6) using the MVAB normal (timing normal).*

[d] *The propagation speed from timing analysis, it is estimated as* $V_f^{'} = V_n / \sin\alpha_2$.

4. Summary and discussion

In this paper, we present a single-point method, based on magnetic field measurements made by spacecrafts, to quantitatively estimate flapping motion parameters of a magnetotail current sheet. Amplitude, wavelength, and propagation velocity can be estimated from our method. For a typical flapping case of the Earth's magnetotail, we demonstrated that our estimated average parameters are well consistent with the multi-point timing analysis of Cluster. Thus, our method could potentially be applied to studying flapping dynamics when multi-point measurements are unavailable, particularly in the case of planetary spacecraft missions.

Building on the single-point method by Rong et al. (2015a), we can now summarize the complete procedure of diagnosing tail flapping motions based on a single-point magnetic field measurement as follows:

1) We set up local coordinate **(L, M, N)** for the current sheet, where the undisturbed current sheet lies in the LM plane, +**L** is basically along the local lobe field pointing earthward, the normal current sheet is along the +**N** direction, and **M**= **L**×**N** points duskward.
2) Given the local coordinate, we fit the magnetic field structure of an undisturbed current sheet to the Harris sheet model, so that the structure of undisturbed current sheet can be roughly obtained.
3) At the crossing of each current sheet, we perform MVAB to calculate the local normal of the current sheet, and check the sequence of calculated parameter k in the local coordinate system. Based on the obtained sequence of k, we can

372 determine the flapping type and the propagation direction of kink-like flapping
373 waves using the technique developed by Rong et al. (2015a).
374 4) With knowledge of the fitted Harris sheet model and the local normal of each
375 current sheet from local coordinate, we can estimate the spatial amplitude of
376 flapping motion via Eq.(4). Based on our diagnosis of flapping types, we can
377 further estimate the wavelength and propagation speed of kink-like flapping
378 waves via Eq. (5) and Eq.(6) respectively.

379 By comparing the inferred propagation speed with the one from timing analysis
380 (see the column of '$V_f^{'}$' in Table 2), which could be seen as the true propagation
381 speed, we find that our estimated speeds at each crossing (see '$V_{f,\,MVAB}$' in Table 2) are
382 not necessarily equal to the speeds estimated by timing analysis, even though the
383 modification of the current sheet normal by the timing normal is considered (see '$V_{f,\,timing}$' in Table 2). The multiple error sources, e.g. uncertainty of the MVAB normal,
385 the irregularity waveform of flapping current sheet, and the temporal variation of
386 undisturbed current sheet etc., may contribute together to affect the accuracy of
387 estimated parameters.

388 Despite a discrepancy with timing analysis at each crossing of the current sheet, the
389 mean propagation speed ($<V_{f,\,MVAB}>\sim$ 32 km/s) is, from our estimation, comparable to
390 the mean propagation speed obtained by timing analysis ($<V_f^{'}>\sim$ 42 km/s). Thus, our
391 single-point method is suitable for calculating average parameters during the whole
392 flapping period, but would probably be unable to estimate such parameters accurately
393 at each crossing of the current sheet.

Acknowledgments

The authors thank the Cluster MAG team for providing the magnetic field data which is accessible at Cluster Science Archive (http://www.cosmos.esa.int/web/csa/access). This work is supported by the Strategic Priority Research Program of Chinese Academy of Sciences (Grant No. XDA17010201), the Key Research Program of the Institute of Geology & Geophysics, CAS (Grant No. IGGCAS- 201904), and the National Natural Science Foundation of China (Grant Nos. 41774188, 41922031, 41874190, and 41525016).

References

Balogh, A., et al. (2001), The Cluster magnetic field investigation: Overview of inflight performance and initial results, Ann. Geophys., 19, 1207–1217.

DiBraccio, G. A., Dann, J., Espley, J. R., Gruesbeck, J. R., Soobiah, Y., Connerney, J. E. P., et al. (2017). MAVEN observations of tail current sheet flapping at Mars. Journal of Geophysical Research: Space Physics, 122, 4308–4324. https://doi.org/10.1002/2016JA023488

Erkaev, N. V., V. S. Semenov, and H. K. Biernat (2007), Magnetic double gradient instability and flapping waves in a current sheet, Phys. Rev. Lett., 99, 235003, doi:10.1103/PhysRevLett.99.235003

Fairfield, D. (1979). On the average configuration of the geomagnetic tail. Journal of Geophysical Research, 84(A5), 1950–1958. https://doi.org/10.1029/JA084iA05p01950

Gao, J. W., Rong, Z. J., Cai, Y. H., Lui, A. T. Y., Petrukovich, A. A., Shen, C., et al. (2018). The distribution of two flapping types of magnetotail current sheet: Implication for the flapping mechanism. Journal of Geophysical Research: Space Physics, 123, 7413–7423. https://doi.org/10.1029/2018JA025695

Golovchanskaya, I. V., and Y. P. Maltsev (2005), On the identification of plasma sheet flapping waves observed by Cluster, Geophys. Res. Lett., 32, L02102, doi: 10.1029/2004GL021552

Harris, E. G. (1962), On a plasma sheet separating regions of oppositely directed magnetic field, Nuovo Cim., 23, 115–121, doi: 10.1007/BF02733547

Harvey, C. C. (1998), Spatial gradients and the volumetric tensor, in Analysis Methods for Multi-Spacecraft Data, edited by G. Paschmann and P. W. Daly, pp. 307–322, Eur. Space Agency, Noordwijk, Netherlands.

Karimabadi, H., W. Daughton, P. L. Pritchett, and D. Krauss-Varban (2003a), Ion-ion kink instability in the magnetotail: 1. Linear theory, J. Geophys. Res., 108(A11), 1400, doi: 10.1029/2003JA010026

Karimabadi, H., P. L. Pritchett, W. Daughton, and D. Krauss-Varban (2003b), Ion-ion kink instability in the magnetotail: 2. Three-dimensional full particle and hybrid simulations and comparison with observations, J. Geophys. Res., 108(A11), 1401, doi: 10.1029/2003JA010109

Lui, A. T. Y., Meng, C.-I. & Akasofu, S.-I. (1978). Wavy nature of the magnetotail neutral sheet. Geophysical Research Letters, 5, 279–282. https://doi.org/10.1029/GL005i004p00279

Petrukovich, A. A., T. L. Zhang, W. Baumjohann, R. Nakamura, A. Runov, A. Balogh, and C. Carr (2006), Oscillations of flux tube slippage in the quiet plasma sheet, Ann. Geophys., 24, 1695–1704

441 Rong, Z. J., C. Shen, A. A. Petrukovich, W. X. Wan, and Z. X. Liu (2010), The
442 analytic properties of the flapping current sheets in the Earth magnetotail, Planet.
443 Space Sci., 58(10), 1215–1229, doi:10.1016/j.pss.2010.04.016
444 Rong, Z. J., S. Barabash, Y. Futaana, G. Stenberg, T. L. Zhang, W. X. Wan, Y. Wei,
445 X.-D. Wang, L. H. Chai, and J. Zhong (2014), Morphology of magnetic field in
446 near-Venus magnetotail: Venus express observations, J. Geophys. Res. Space
447 Physics, 119, 8838–8847, doi: 10.1002/2014JA020461
448 Rong, Z. J., Barabash, S., Stenberg, G., Futaana, Y., Zhang, T. L., Wan, W. X., et al.
449 (2015a). Technique for diagnosing the flapping motion of magnetotail current
450 sheets based on single-point magnetic field analysis. Journal of Geophysical
451 Research: Space Physics, 120, 3462–3474.https://doi.org/10.1002/2014ja020973
452 Rong, Z. J., Barabash, S., Stenberg, G., Futaana, Y., Zhang, T. L., Wan, W. X., et al.
453 (2015b). The flapping motion of the Venusian magnetotail: Venus Express
454 observations. Journal of Geophysical Research: Space Physics, 120, 5593–5602.
455 https://doi.org/10.1002/2015ja021317
456 Rong, Z. J., Cai, Y. H., Gao, J. W., Lui, A. T. Y., Shen, C., Petrukovich, A. A., et al.
457 (2018a). Cluster observations of a dispersive flapping event of magnetotail current
458 sheet. Journal of Geophysical Research: Space Physics, 123, 5571–5579.
459 https://doi.org/10.1029/2018JA025196
460 Rong, Z. J., et al. (2018b). The magnetic field structure of Mercury's magnetotail.
461 Journal of Geophysical Research: Space Physics, 123, 548–566.
462 https://doi.org/10.1002/2017JA024923
463 Runov, A., et al. (2005), Electric current and magnetic field geometry in flapping
464 magnetotail current sheets, Ann. Geophys., 23, 1391–1403.
465 Sergeev, V., Angelopoulos, V., Carlson, C., & Sutcliffe, P. (1998). Current sheet

466 measurements within a flapping plasma sheet. Journal of Geophysical Research,
467 103, 9177–9187. https://doi.org/10.1029/97JA02093
468 Sergeev, V., et al. (2003), Current sheet flapping motion and structure observed by
469 Cluster, Geophys. Res. Lett., 30(6), 1327, doi: 10.1029/2002GL016500
470 Sergeev, V., A. Runov, W. Baumjohann, R. Nakamura, T. L. Zhang, A. Balogh, P.
471 Louarn, J.-A. Sauvaud, and H. Reme (2004), Orientation and propagation of current
472 sheet oscillations, Geophys. Res. Lett., 31, L05807, doi: 10.1029/2003GL019346
473 Shen, C., Rong, Z. J., Li, X., Dunlop, M., Liu, Z. X., Malova, H. V., et al. (2008).
474 Magnetic configurations of tail tilted current sheet. Annales de Geophysique,
475 26(11), 3525–3543. https://doi.org/10.5194/angeo-26-3525-2008
476 Sitnov, M. I., M. Swisdak, P. N. Guzdar, and A. Runov (2006), Structure and
477 dynamics of a new class of thin current sheets, J. Geophys. Res., 111, A08204, doi:
478 10.1029/2005JA011517
479 Sonnerup, B. U. Ö., and M. Scheible (1998), Minimum and maximum variance
480 analysis, in Analysis Methods for Multi-Spacecraft Data, edited by G. Paschmann
481 and P. W. Daly, pp. 185–220, Eur. Space Agency, Noordwijk, Netherlands.
482 Speiser, T. W., & Ness, N. F. (1967). The neutral sheet in the geomagnetic tail: Its
483 motion, equivalent currents, and field-line reconnection through it. Journal of
484 Geophysical Research, 72, 131–141. https://doi.org/10.1029/JZ072i001p00131
485 Toichi, T., & Miyazaki, T. (1976). Flapping motions of the tail plasma sheet induced
486 by the interplanetary magnetic field variations. Planetary and Space Science, 24,
487 147-159, https://doi.org/10.1016/0032-0633(76)90102-1
488 Thompson, S. M. et al. (2005). Dynamic Harris current sheet thickness from Cluster
489 current density and plasma measurements, J. Geophys. Res., 110, A02212, doi:
490 10.1029/2004JA010714

491 Volwerk, M., André, N., Arridge, C. S., Jackman, C. M., Jia, X., Milan, S. E., et al.
492 (2013). Comparative magnetotail flapping: An overview of selected events at Earth,
493 Jupiter and Saturn. Annales de Geophysique, 31(5), 817–833.
494 https://doi.org/10.5194/angeo-31-817-2013
495 Wu, M. Y., Q. Lu, M. Volwerk, Z. Vörös, X. Ma, and S. Wang (2016), Current sheet
496 flapping motions in the tailward flow of magnetic reconnection, J. Geophys. Res.
497 Space Physics, 121, 7817–7827, doi: 10.1002/2016JA022819
498 Zelenyi, L. M., A. V. Artemyev, A. A. Petrukovich, R. Nakamura, H. V. Malova, and V.
499 Y. Popov (2009), Low frequency eigenmodes of thin anisotropic current sheets and
500 Cluster observations, Ann. Geophys., 27, 861–868.
501 Zhang, C., Rong, Z. J., Gao, J. W., Zhong, J., Chai, L. H., Wei, Y., et al. (2020). The
502 flapping motion of Mercury's magnetotail current sheet: MESSENGER
503 observations. Geophysical Research Letters, 47, e2019GL086011.
504 https://doi.org/10.1029/2019GL086011
505 Zhang, T. L., W. Baumjohann, R. Nakamura, A. Balogh, and K.-H. Glassmeier (2002),
506 A wavy twisted neutral sheet observed by Cluster, Geophys. Res. Lett., 29(19),
507 1899, doi: 10.1029/2002GL015544
508 Zhang, T. L., Nakamura, R., Volwerk, M., Runov, A., Baumjohann, W., Eichelberger,
509 H. U., et al. (2005). Double Star/Cluster observation of neutral sheet oscillations on
510 5 August 2004. Annales Geophysicae, 23(8), 2909–2914.
511 https://doi.org/10.5194/angeo‐23‐2909‐2005
512 Zhang, T. L. et al. (2006), A statistical survey of the magnetotail current sheet, Adv.
513 Space Res., 38, 1834–1837, doi: 10.1016/j.asr.2006.05.009